DOI 10.1007/s12541-009-0029-9

Study of Dynamic Crack Propagation in 3PB Steel Specimens Loaded by Impact

Jae-Ung Cho[1], Chong-Du Cho[2] and Moon-Sik Han[3,#]

1 Faculty of Mechanical and Automotive Engineering, Kongju University, 275 Budae-dong, Cheonan, Chungnam, Korea, 330-717
2 Faculty of Mechanical and Automotive Engineering, Inha University, 253 Yonghyun-dong, Nam-gu, Incheon, Korea, 402-751
3 Faculty of Mechanical and Automotive Engineering, Keimyung University, 2800 Dalgubeoldaero, Dalseo-Gu, Daegu, Korea, 704-701
Corresponding Author / E-mail: sheffhan@kmu.ac.kr, TEL: +82-53-580-5255, FAX: +82-53-580-6935

KEYWORDS: Ductile steel, Newly designed 3PB specimens, Moiré interference patterns, Crack propagation, Crack tip opening displacement, Mid-support force

Crack propagation in ductile steel was investigated using impact-loaded three-point bending (3PB) specimens. Results from experiments and numerical simulations were compared. The specimens were 320 x 75 mm by 10 mm thick. A new 3PB specimen design with reduced width at the ends was developed to avoid the influence of uncertain boundary conditions at the impact heads. One static and two dynamic tests with impact velocities of 30.2 and 45.2 m/s were performed. High-speed photography was used to obtain crack growth and crack tip opening displacement data. Moiré interference patterns were used to directly measure the relative rotation of the two specimen halves. Shear lip fracture surfaces were obtained for all three loading conditions. The experiments indicated no, or only a slight, loading rate influence on the crack propagation.

Manuscript received: September 26, 2008 / Accepted: December 1, 2008

1. Introduction

This investigation studied criteria for crack initiation and propagation in ductile steel three-point bending (3PB) specimens loaded by impact. First, a preparatory theoretical study was performed through experiments and numerical simulations of dynamic crack initiation in microalloyed manganese steel.[1-4] Experiments were then carried out on 18 mm thick 3PB specimens.[5] Starting with a prefabricated fatigue quarter-width crack, the specimens were tested at impact velocities of 30.2 and 45.2 m/s in the acceleration track test facility depicted in Figure 1. The 3PB sample was loaded by striking it at the ends with a U-shaped hammer to minimize translation of the specimen midpoint area, thereby optimizing the possibility of using high-speed photography to record the crack propagation through the specimen.

The specimen behavior is greatly influenced by the boundary conditions between the hammer and the specimen at the impact points.[3, 6-9] The ductile specimen deforms plastically where it is hit by the impact heads, particularly at higher impact velocities. The shaped heads form circular indents, which in turn work as guides for successive specimen deformation. Mechanical locking at these indents and friction between the impact heads and the specimen have a pronounced influence on the response of the specimen. This unwanted compressive loading of the crack plane is obtained in the initial phase of the impact.

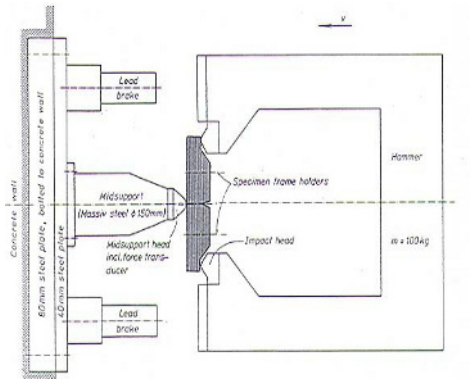

Fig. 1 Experimental setup

This study examined the behavior of the material, focusing on finding the conditions to control shear lip formation. In order to obtain systematic data for crack initiation and crack propagation, the investigation concentrated on the influence of the impact velocity on the shear mode behavior in dynamic loading. At high

impact velocities of 30.2 and 45.2 m/s, ductile shear lips are almost always found at the outer parts of the fracture surfaces.[10] Therefore, these impact velocities were applied to study the purely ductile specimen behavior. The total shear lip thickness obtained at a 45.2 m/s impact velocity was about 10 mm. The specimen thickness was therefore reduced to 10 mm to suppress the cleavage fracture mode in the specimens' interior. These dynamic experiments were performed in the acceleration test facility, where a U-shaped hammer with two hardened and tempered cylindrical contact-surface impact heads was accelerated to the prescribed velocity and hit the 3PB specimen at its ends. These dynamic experiments were carried out at 18℃. A quasi-static test was also performed, with a midpoint loading at a velocity of 50 mm/min.

2. Experiments

The initial part of the crack was milled, and then the specimen was subjected to 3PB for about 40,000 cycles to produce a crack with a length one-quarter the specimen height. The material used was ductile at static loading. The chemical composition is listed in Table 1 for the Mn-alloyed, normalized steel specimen (Swedish notation: SIS2134), and the results from a static tensile test are shown in Figure 2.

Table 1 Chemical composition

Components (wt%)						
C	Si	Mn	P	S	Al	Nb
0.14	0.30	1.41	0.014	0.011	0.045	0.030
V	N	Mo	Cu	Cr	Ni	
0.008	0.005	0.004	0.009	0.02	0.04	

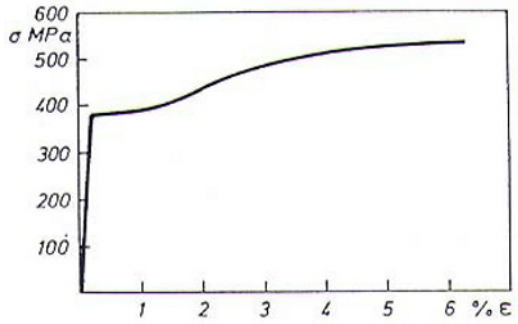

Fig. 2 Static tensile test diagram (engineering strain vs. stress)

The dynamic experiments were recorded using high-speed photography, from which detailed measurements of crack propagation and crack tip opening displacements (CTOD) were made.[11] The relative rotation was calculated from the distance between the Moiré interference pattern lines obtained from the high-speed photographs. An ordinary 24 × 36 mm negative format camera was used to record the crack propagation during static tests. As depicted in Figure 1, a force transducer was incorporated in the mid-support. The impact time was detected using strain gauges attached where the hammer hits the ends of the specimen. A Cordin 377 high-speed camera operating at 100,000 frames per second for the 30.2 m/s impact tests and at 160,000 frames per second for the 45.2 m/s impact tests was used in the dynamic experiments. There were no exposure problems using the standard Cordin flash unit placed 0.5 m away and Kodak TMAX 3200 film. Moiré interference patterns were obtained between the grid milled on the specimen surface and the reference grid 3 mm above the specimen.[12,13] The reference grid, copied onto a transparent self-adhesive plastic sheet, was mounted on a PMMA plate. There was a rectangular hole in the reference grid and plate to expose the first 20 mm of the fracture area.

The slanted interference pattern signified a frequency mismatch between the reference and specimen grids. The pitch difference was due to the distance differences from the two grids to the camera. The specimen pitch was measured with a microscope. The interference pattern pitch was then measured from the high-speed photographs, and the relative rotation of the two specimen halves was calculated from the following relationship:

$$\cos\frac{\varphi}{2}=\frac{\delta_1}{2\delta_2}\left\{1+\left(\frac{\delta_1}{\delta_2}\right)^2-\left(\frac{\delta_2}{l}\right)^2\right\} \tag{1}$$

where:
ρ: relative rotation
δ_1: reference grid pitch
δ_2: specimen grid pitch
l: interference pattern pitch

This relationship is valid provided that there is no change in the specimen grid or reference grid pitch. Using this relationship, the effective reference grid pitch versus the specimen grid was calculated with the interference pattern pitch measured at the beginning of the recording when the relative rotation $\rho = 0$.

3. Results and Discussion

3.1 Comparison of conventional and newly designed specimens

The two specimen halves rotated approximately around the specimen midpoint (marked with an X in Figure 3) if free motion of the specimen, relative to the impact heads was not allowed. However, the distance between the impact heads was fixed. The large plastic deformation of the specimen caused by the circular impact heads in the initial phase of the impact acted as a mechanical guide for the successive loading of the specimen, thereby moving the center of the relative rotation closer to the crack mouth.

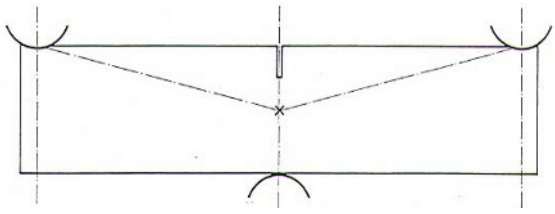

Fig. 3 Conventional 3PB specimen design. Rotation of the point lines indicate the relative motion of the specimen halves

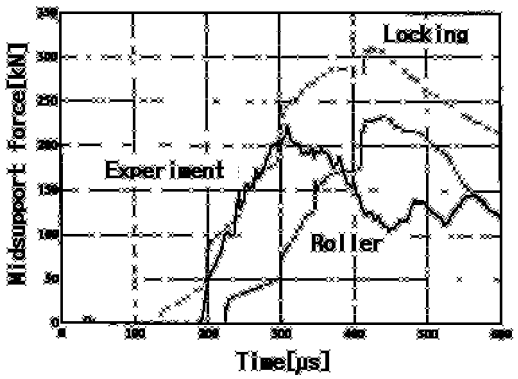

Fig. 4 Comparison between experiments and simulations of the mid-support force versus time for a 30.2 m/s impact velocity on a conventional specimen. Experiment: solid line; simulations – roller: dotted line, locking: dashed line

A great difference in specimen behavior for the two extremes at the impact heads for locking and roller conditions was demonstrated by the compressive force induced on the crack plane.[6] Plots of the mid-support force versus time for an impact velocity of 30.2 m/s are compared for the conventional and the newly designed specimens in Figures 4 and 5.

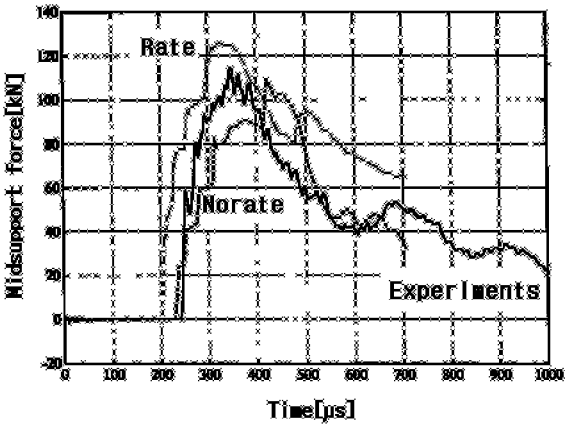

Fig. 5 Comparison between experiments and simulations of the mid-support force versus time for 30.2 m/s impact velocity on the newly designed specimen. Experiment: solid line; simulations – no rate: dotted line, rate: dashed line

As shown in Figure 4, the influence of possible friction forces between the support points and the specimen was investigated by examining the extreme cases of loose roller and completely locking supports. The mid-support forces in the simulations of conventional specimens were different for the roller and locking condition than those of the experiment. Therefore, it was difficult to reconcile the simulations with the experimental data.

Simulations were also performed with rate dependent material properties according to the one-dimensional Malvern viscoplastic model:[13]

$$\dot{\varepsilon}^{vp} = \beta(\frac{\sigma}{\sigma_y} - 1)^n \tag{2}$$

where

$\dot{\varepsilon}^{vp}$: plastic strain
σ: stress
σ_y: yield stress
β, η: viscoplastic parameters

Figure 5 also shows a simulation of the mid-support force as a function of time for the 30.2 m/s impact velocity test. However, here the viscoplastic parameters $\beta = 4000$ and $n = 2$ were selected to yield a moderate viscoplastic influence. The notation 'Rate' and 'No rate' indicate the results from simulations with and without rate-dependent material properties.

In Figure 5, with the newly designed specimen, the experimental data agreed with the simulations for the mid-support forces both with and without the rate-dependent material properties. Therefore the crack was initially closed when the conventional 3PB specimen design was used.

Since conditions at the impact heads are difficult to quantify, the specimen was redesigned to avoid compressive loading during the initial phase of the impact using the geometry and dimensions shown in Figure 6, with the width reduced at the ends. The relative motion of the two specimen halves approximately followed the motion of the two marked point lines. The impact points and the center of rotation of the two specimen halves lay almost on a straight line when there was no initial compressive loading of the crack tip. The specimen width could have been reduced further at the impact points so that specimen midpoint would fall on a straight line.

Figure 6 also indicates the longitudinal grid milled on the entire upper specimen surface for direct Moiré interference pattern measurement of the relative rotation of the two specimen halves. The force transducer was calibrated for static loading up to 350 kN, and for dynamic loading by using stress-pulses from a 1-m long circular bar hitting the transducer longitudinally.[12] The mid-support reaction force was determined from the strain gauge recordings of the reaction head deformation. As also shown in Figure 6, two strain gauges were mounted at the specimen ends, about 25 mm from the impact points, to detect the time of impact. The dilatational stress wave velocity in steel is about 6 mm/μs. First detection at this position was therefore obtained about 4 μs after impact. Endevco HBM 3020 C bridge amplifiers were used for the strain gauge channels and the signals were recorded on two Nicolet (2090 and 3091) transient recorders using a 1-MHz sampling frequency. One channel from each of the transient recorders was used for the flash-start light detector to calibrate the photographs

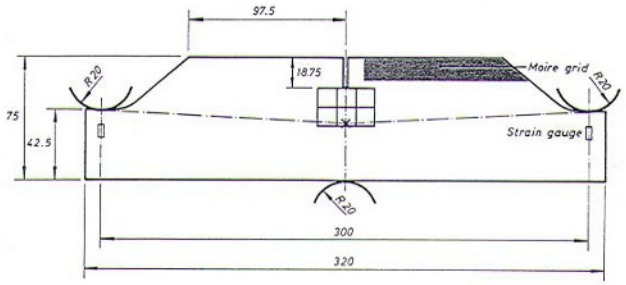

Fig. 6 Dimensions (in mm) of the newly designed 3PB specimen

and the electronic recordings. The trigger circuit for the flash and the transient recorders was activated at a hammer position about 5 mm in front of the specimen. The hammer speed was obtained from measuring the time to travel 200 mm.

3.2 Comparison of the newly designed specimens

We examined three impact cases: a static test (midpoint loading with a displacement rate of 50 mm/min), and dynamic tests at 30.2 m/s and 45.2 m/s impact velocities. Photographs from the static test are presented in Figure 7, and the high-speed photographs from the dynamic tests are shown in Figures 8 and 9.

Fig. 7 Photographs from the static test

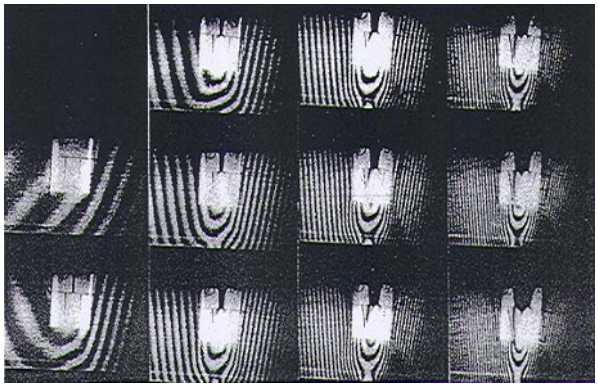

Fig. 8 High-speed photographs from the 30.2 m/s impact velocity test

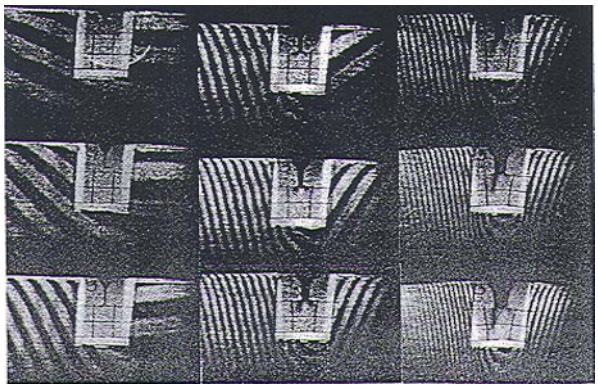

Fig. 9 High-speed photographs from the 45.2 m/s impact velocity test

No qualitative differences in specimen behavior were found among the three cases. Ductile surfaces with shear lips of 45 degrees were obtained throughout the specimens with the exception of a small triangular area with its base on the fatigue pre-crack. No sign of a ductile to brittle crack surface transition was observed.

3.2.1 Crack propagation

The possible influence of the loading rate can be observed when the results are presented as a function of the relative rotation of the two specimen halves. Figure 10 shows the crack propagation for the static and two dynamic tests. Due to the limited resolution of the high-speed photographs, the crack propagation, corresponding to blunting at the crack tip, can only be observed in the static experiment photographs. However, it is most probable that such blunting also occurred during the dynamic tests. The result of removing the blunting part of the static crack propagation is shown in Figure 11. The diagrams for the three loading tests were close to each other, with a slightly earlier crack propagation for the 45.2 m/s dynamic test compared to the static and 30.2 m/s dynamic tests. This result indicates that there was no, or only a minor, influence on the crack propagation properties from the loading rate.

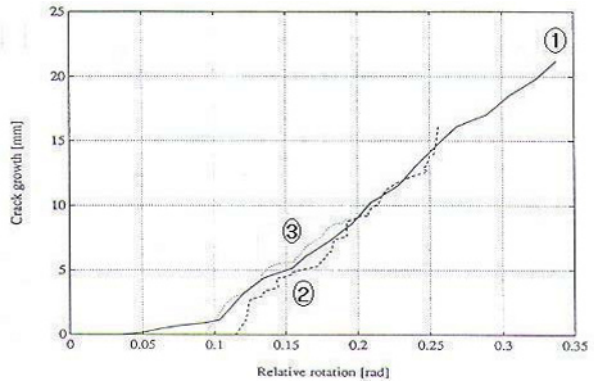

Fig. 10 Crack propagation for the static and two dynamic tests as a function of the relative rotation (①: static test, ②: dynamic test, 30.2 m/s impact velocity, ③: dynamic test, 45.2 m/s impact velocity)

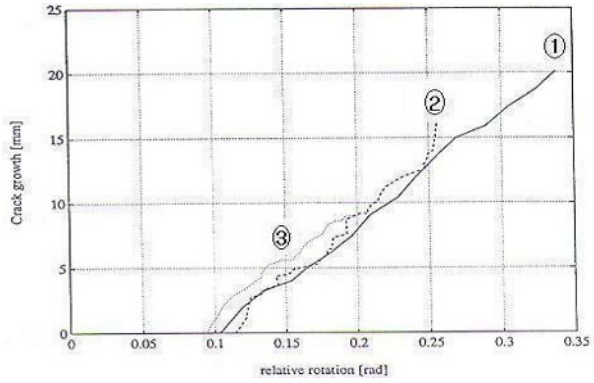

Fig. 11 Crack propagation for the static and two dynamic tests as a function of the relative rotation (①: static test (blunting part of the crack propagation removed), ②: dynamic test, 30.2 m/s impact velocity, ③: dynamic test, 45.2 m/s impact velocity)

3.2.2 Crack tip opening displacement

The crack tip opening displacement, CTOD, is presented as a function of relative rotation in Figure 12. Here, the results of the static and two dynamic tests all fell close to each other. The crack propagation became faster with a higher loading rate. However, we concluded that regardless of the loading rate, there was no, or only a minor, influence from the loading rate on the crack growth and crack tip opening displacement as a function of relative rotation.

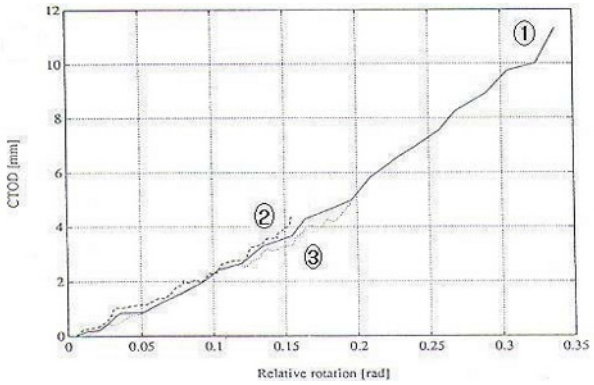

Fig. 12 Crack tip opening displacement for the static and two dynamic tests as a function of the relative rotation (①: static test, ②: dynamic test, 30.2 m/s impact velocity, ③: dynamic test, 45.2 m/s impact velocity)

3.2.3 Mid-support force

The mid-support force is presented in Figure 13 as a function of the relative rotation. The largest mid-support force for the static and two dynamic tests was observed for the 30.2 m/s impact velocity at a relative rotation of 0.1 rad.

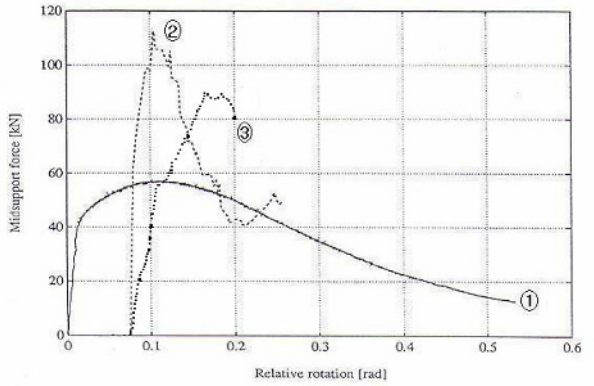

Fig. 13 Mid-support force for the static and two dynamic tests as a function of the relative rotation (①: static test, ②: dynamic test, 30.2 m/s impact velocity, ③: dynamic test, 45.2 m/s impact velocity)

4. Conclusions

Our experiments investigating the nonlinear plastic behavior for impact loaded 3PB specimens yielded the following conclusions.

1. The dynamic 45.2 m/s test exhibited a slightly earlier crack propagation than the static and dynamic 30.2 m/s tests. The crack growth and crack tip opening displacement in the dynamic tests for loading rates of 30.2 m/s and 45.2 m/s as a function of the relative rotation followed the curve of the static test.
2. The loading rate had no, or only a minor, influence on the crack growth and crack tip opening displacement as a function of the relative rotation.
3. The crack tip opening displacement could be presented as a function of the relative rotation.
4. Among the static and two dynamic cases, the largest mid-support force occurred with an impact velocity of 30.2 m/s at a relative rotation of 0.1 rad.

ACKNOWLEDGEMENT

This work was supported by Korea Science & Engineering Foundation through the Joint Research Program (Grant No. F01-2008-000-10017-0).

REFERENCES

1. Kao, H. R., "The dynamic behavior of the middle or side impact loaded 3-point bend specimen," Lund Institute of Technology, Technical Report LUTFD2 TFHF-3034, pp. 1-18, 1990.
2. Van Elst, H. G., "Assessment of dynamic fracture propagation resistance at instrumented high velocity gasgun impact tests on SENB-Specimens," ICF, Vol. 6, No. 5, pp. 3089-3097, 1984.
3. Chae, J. S., Park, T. W. and Kim, J., "Dynamic Analysis of A Flexible Multibody System," Int. J. Precision Engineering and Manufacturing, Vol. 6, No. 4, pp. 21-25, 2005.
4. Son, I. S., Cho, J. R. and Yoon, H. I., "Effects of a Moving Mass on the Dynamic Behavior of Cantilever Beams with Double Cracks," Int. J. Precision Engineering and Manufacturing, Vol. 9, No. 3, pp. 33-39, 2008.
5. Nakamura, T., Shih, C. F. and Freund, L. B., "Analysis of a dynamically loaded three point bend ductile fracture specimen," Engineering Fracture Mechanics, Vol. 25, No. 3, pp. 323-339, 1986.
6. Bergmark, A. and Kao, H. R., "Dynamic crack initiation in 3PB ductile steel specimens," Lund Institute of Technology, Technical Report LUTFD2 TFHF-3041, pp. 1-23, 1991.
7. Jang, I. S. and Chae, D. B., "The derivation of simplified vehicle body stiffness equation using collision analysis," Trans. of KSAE, Vol. 8, No. 4, pp. 177-185, 2000.
8. Kanninen, M. F. and Popelar, C. H., "Advanced Fracture Mechanics," Oxford Engineering Science Series 15, 1985.
9. Zhang, J. F., Wang, B. and Dong, S., "Analysis of Factors Impacting Atmospheric Pressure Plasma Polishing," Int. J. Precision Engineering and Manufacturing, Vol. 9, No. 2, pp. 39-43, 2008.
10. Huang, C., Zhu, H., Lu, X., Li, Q. and Che, C., "Transition Mechanism from Brittle Fracture to Ductile Shear when Machining Brittle Materials with an Abrasive Waterjet," Int. J. Precision Engineering and Manufacturing, Vol. 9, No. 2, pp. 11-17, 2008.
11. Knott, J. F., "Fundamentals of Fracture Mechanics," Butterworth, 1973.

12. Aref, H., "Academic Press - Vol. 41," Advances in Applied Mechanics, 2006.

13. Malvern, L. E., "The propagation of longitudinal waves of plastic deformation in a bar of material exhibiting a strain-rate effect," J. Appl. Mech., Vol. 18, pp. 203-208, 1951.